Available online at www.sciencedirect.com
ScienceDirect
Journal of the European Ceramic Society 27 (2007) 2377–2383
www.elsevier.com/locate/jeurceramsoc

Finite element analysis of sintering deformation using densification data instead of a constitutive law

Sasan Kiani [a], Jingzhe Pan [b,*], Julie A. Yeomans [a], Magali Barriere [c], Philippe Blanchart [c]

[a] *School of Engineering, University of Surrey, Guildford GU2 7XH, UK*
[b] *Department of Engineering, University of Leicester, Leicester LE1 7RH, UK*
[c] *Ecole Nationale Supérieure de Céramique Industrielle (ENSCI), 43-73 Avenue Albert Thomas, 87605 Limoges Cedex, France*

Received 22 April 2006; received in revised form 23 August 2006; accepted 25 August 2006
Available online 6 October 2006

Abstract

Various forms of constitutive laws have been developed for use in the finite element analysis of sintering deformation. Some of these were based on micromechanical models and others were based on empirical fitting of experimental data. The mechanism-based constitutive laws differ from each other widely and it can be difficult to know which one to use. On the other hand, obtaining fitting functions for an empirical constitutive law is very time consuming. In this paper, an empirical finite element method is presented which does not require a constitutive law; rather the densification data (density as a function of time) is used to predict sintering deformation. The densification data can be obtained by sintering a relatively small number of samples of the powder or derived from the master sintering curve. Different sintering mechanisms and non-linearity pose no difficulty to the method. The method is, however, limited to pressureless sintering. To verify the densification-based finite element method, three case studies are presented. The numerical predictions were compared with experimental measurement for two different cases. It is shown that the accuracy of the prediction is well within the experimental uncertainties and comparable to previous finite element analyses using full constitutive laws.

Keywords: Sintering; Modelling

1. Introduction

Most of ceramic products are made by sintering, a process in which compacts of fine powder are fired and consolidated. To achieve full density the products often experience large shrinkages, typically of the order of 20–30%, during the firing process. Dimensional control is therefore a critical issue in sintering technology because post-processing is expensive and can introduce damage. The large shrinkage also leads to residual stresses in an anisotropic system, e.g. multilayer and functionally graded materials. The temporal evolution of shape, density profile and residual stresses during sintering can be predicted using the classical finite element method. The key input in a finite element analysis is the constitutive law which links strain rates with stresses. Reviews of the constitutive laws and finite element analysis of sintering have been provided by Cocks,[1] Olevsky[2] and Pan.[3]

Two approaches have been adopted to establish the constitutive laws. The first approach is to use micromechanical models in which a controlling sintering mechanism is assumed (for example, grain-boundary diffusion,[4–6] viscous flow[2] or liquid phase sintering[7,8]) and a simplification to the microstructure is made (densely packed uniform spherical particles[4] or a three-dimensional array of tetrakaidecahedra grains,[5,6] for example). Matter redistribution during sintering is typically realised by diffusion processes, which are very sensitive to the chemical composition and the shortest diffusion distance available. A small variation in the chemical impurity can change the diffusion coefficient by several orders of magnitude. Microstructral features such as particle agglomeration, large pores and particle size distribution always exist in a powder compact. However, the current generation of constitutive laws does not take the chemical effect into account because of the uncertainty in knowing the

* Corresponding author. Tel.: +44 116 223 1092.
E-mail address: jp165@le.ac.uk (J. Pan).

0955-2219/$ – see front matter © 2006 Elsevier Ltd. All rights reserved.
doi:10.1016/j.jeurceramsoc.2006.08.019

exact chemical composition and homogeneity. The substructures in a powder compact are also ignored because of the mathematical difficulty in obtaining an analytical solution for such a microstructure. Consequently the mechanism-based constitutive laws differ from each other widely, each depending on its assumed sintering mechanism and microstructure.[9] It is often difficult to know which mechanism-based constitutive law to choose in a sintering analysis. The second approach to establish a constitutive law is to fit the experimental data directly. The work by Bouvard and his co-workers[10–12] provides a recent example. This is however an expensive and time consuming exercise; in the experiment a force has to be applied to the sample at the sintering temperature. Furthermore, in order to determine the parameters in a grain growth law, a series of interrupted sintering tests need to be performed and the grain-size of each sample determined which is yet another expensive and time consuming exercise. These difficulties have severely limited industry from using the finite element analysis in developing sintered products.

Several researchers have attempted to predict sintering deformation using fewer data than a full constitutive law. Tsvelikh et al.[13] suggested an empirical finite element analysis. Ozkan and Briscoe[14,15] integrated the densification rate equation for a cylinder in which there was a density distribution. DiAntonio et al.[16] used data from master sintering curves and compatibility conditions for a multilayer system. Whilst, there is a lack of theoretical grounding in these previous efforts and consequently the numerical schemes are arbitrary, this body of work was the inspiration behind the current paper. Here, a finite element scheme is presented that requires only the densification data (density as a function of time) to predict the temporal evolution of sintering deformation. In the terminology of continuum solid mechanics, the proposed finite element method satisfies the compatibility, equilibrium conditions and partially the constitutive law. From the point of view of a user of a commercial finite element package, the method requires a unity material matrix and a user-defined force matrix into which the densification data is input. The actual sintering mechanisms and any non-linearity in the constitutive law are irrelevant to the method. However, the method is only valid for pressureless sintering. In the following discussions, the method is referred to as the densification-based finite element method (DFEM). Three case studies are presented in order to verify the DFEM.

2. Formulation of densification-based finite element method

In the finite element model for sintering the elastic deformation is assumed to be small and thus it is ignored, and the porous material is treated as a viscous continuum solid. Using the direct Euler scheme for time integration, at each time-step the velocity field of a sintering body is obtained in its current configuration and then the nodal coordinates of the finite element mesh are updated. The correct velocity field must satisfy four conditions: (a) compatibility, (b) equilibrium, (c) boundary conditions and (d) constitutive law. The aim here is to develop an approximate finite element method for which only the densification data are available. In a general problem of stress analysis this is not possible; a full constitutive law is always needed or the finite element analysis is not possible. In the special case of pressureless sintering, it will be shown that a solution that satisfies conditions (a–c) and partially (d) provides a very good approximation to the exact solution which satisfies all the four conditions. The densification-based finite element method can be formulated from two different angles: (a) using the virtual power principle or (b) using the weighted residual error method.

2.1. DFEM based on the virtual power principle

In a finite element formulation using the velocity field as its basic variable, the compatibility condition is guaranteed by representing the velocity field using appropriate shape functions and by calculating the strain rates from the velocity field using the relationship

$$\dot{\varepsilon}_{ij} = \frac{1}{2}\left[\frac{\partial \dot{u}_i}{\partial x_j} + \frac{\partial \dot{u}_j}{\partial x_i}\right], \tag{1}$$

in which $\dot{\varepsilon}_{ij}$ represents the strain rate tensor, $\dot{u}_i$ the velocity field and x_i is the Lagrange coordinate. The velocity boundary conditions are satisfied by setting the nodal velocities on the boundary to their prescribed values. The equilibrium condition is equivalent to the principle of virtual power, which states that

$$\int_V \sigma_{ij}\,\delta\dot{\varepsilon}_{ij}\,\mathrm{d}V = 0, \tag{2}$$

in which σ_{ij} represents the stress tensor and $\delta\dot{\varepsilon}_{ij}$ represents the virtual variation of the strain rates which must satisfy the compatibility and the velocity boundary conditions. The integration is over the entire sintering body.

Although the DFEM is not limited to linear constitutive laws, it is easier to follow the assumptions made by demonstrating it using a linear constitutive law:

$$\dot{\varepsilon}_{ij} = \frac{s_{ij}}{2\eta_S} + \frac{\sigma_m}{3\eta_B}\delta_{ij} - \frac{\sigma_s}{3\eta_B}\delta_{ij}, \tag{3}$$

in which σ_m represents the mean stress, σ_s the sintering potential, η_S the shear viscosity, η_B the bulk viscosity, δ_{ij} the Kronecker delta function and s_{ij} is the devitoric stress tensor which is defined as

$$s_{ij} = \sigma_{ij} - \sigma_m\delta_{ij}. \tag{4}$$

It can be seen that the strain rates given by Eq. (3) contain three terms. The first term represents the shear deformation, the second term represents the volume change resulting from the mean stress and the third term represents the volume change due to the sintering potential. A sintering body of any shape made of uniform material deforms by the third term alone if the body is unconstrained and no external force is applied. In the following discussion, the third term is referred to as:

$$\dot{\varepsilon}_{exp} = -\frac{\sigma_s}{3\eta_B} = -\frac{\dot{D}}{3D}, \tag{5}$$

in which D represents the relative density. $\dot{\varepsilon}_{exp}$ can be obtained from free sintering experiment using uniform samples or derived from a master sintering curve.[17]

To avoid using the full constitutive law, the second term is dropped from Eq. (3), i.e. it is assumed that σ_m is much smaller than σ_s such that the volume change is due to the sintering potential alone. The constitutive law then becomes

$$\dot{\varepsilon}_{ij} = \frac{s_{ij}}{2\eta_S} + \dot{\varepsilon}_{exp}\delta_{ij}. \tag{6}$$

Using Eq. (6) in Eq. (2) and noticing that $\sigma_m = 0$ gives

$$\int_V \eta_S(\dot{\varepsilon}_{ij} - \dot{\varepsilon}_{exp}\delta_{ij})\,\delta\dot{\varepsilon}_{ij}\,dV = 0. \tag{7}$$

The conditions for Eq. (7) to be valid can be further understood by examining the extract virtual power principle. Eq. (3) can be rewritten as

$$\sigma_{ij} = \lambda\dot{\varepsilon}_{kk}\delta_{ij} + 2\eta_S\dot{\varepsilon}_{ij} - \sigma_s\delta_{ij}, \tag{8}$$

in which $\lambda = (\eta_B - 2\eta_S)/3$, which is known as Lame constant. Substituting Eq. (8) into Eq. (2) gives

$$\int_V 2\eta_S(\dot{\varepsilon}_{ij} - \dot{\varepsilon}_{exp}\delta_{ij})\,\delta\dot{\varepsilon}_{ij}\,dV + \int_V \lambda(\dot{\varepsilon}_{kk} - 3\dot{\varepsilon}_{exp})\,\delta\dot{\varepsilon}_{kk}\,dV = 0. \tag{9}$$

The validity of Eq. (7) is therefore subject to the condition that the second term in Eq. (9) vanishes independently. For early stage sintering, the viscous Poisson's ratio is almost zero leading to $\lambda \approx 0$. This is not true for later stage of sintering. A strong condition for Eq. (7) to be valid is that $\dot{\varepsilon}_{kk} \approx 3\dot{\varepsilon}_{exp}$, i.e. the volumetric strain rate is not affected by the local state and always takes the value of $3\dot{\varepsilon}_{exp}$ as if the material is freely sintered. In fact this condition only needs to be satisfied in the sense of integration.

The shear viscosity η_S can be eliminated from Eq. (7) by assuming that the shear viscosity is uniform within a powder compact, then the virtual power principle can be written as

$$\int_V (\dot{\varepsilon}_{ij} - \dot{\varepsilon}_{exp}\delta_{ij})\,\delta\dot{\varepsilon}_{ij}\,dV = 0. \tag{10}$$

Eq. (10) is the basis for the densification-based finite element method. The only experimental data required by Eq. (10) is $\dot{\varepsilon}_{exp}$ as defined by Eq. (5). The assumption of a uniform η_S makes the DFEM an empirical method as η_S depends on relative density and grain-size and is not exactly uniform if either the density or grain-size varies from location to location in a sintering component.

Following the standard finite element procedure,[18] the velocity field $\dot{u}_i$ is approximated using a set of finite element shape functions and the strain rates $\dot{\varepsilon}_{ij}$ are calculated using Eq. (1). Writing the results in the matrix form, gives

$$[\dot{\varepsilon}]_e = [B][\dot{u}]_e \tag{11}$$

in which e indicates that the matrixes are defined for the eth element, $[B]$ a matrix of known functions of location calculated from the shape functions and $[\dot{u}]_e$ represents the vector of nodal velocities for the eth element. Substituting expression (11) into (10) gives

$$\sum_{\text{elements}} \delta[\dot{u}]_e^T\{[K]_e[\dot{u}]_e - [F]_e\} = 0 \tag{12}$$

in which

$$[K]_e = \int_{V_e} [B]^T[B]\,dV \tag{13}$$

and

$$[F]_e = \int_{V_e} [B]^T[\dot{\varepsilon}_{exp} \quad \dot{\varepsilon}_{exp} \quad \dot{\varepsilon}_{exp} \quad 0 \quad 0 \quad 0]\,dV \tag{14}$$

For Eq. (12) to be true for any arbitrary $\delta[\dot{u}]$, we must have

$$\sum_{\text{elements}} \{[K]_e[\dot{u}]_e - [F]_e\} = 0 \tag{15}$$

Eq. (15) represents a set of linear simultaneous equations in terms of the nodal velocities, which can be solved using a standard solver. It is useful to recognise that the elemental viscosity matrix defined by Eq. (13) is equivalent to simply setting the material matrix in the usual finite element analysis as a unit matrix.

2.2. DFEM based on the weighted residual error method

The DFEM is not limited to the linear constitutive law. In a free sintering of a uniform and unconstrained component (of any complicated shape), the strain rates everywhere in the component are given exactly by

$$\dot{\varepsilon}_{ij} = \dot{\varepsilon}_{exp}\delta_{ij}. \tag{16}$$

If a component is non-uniform or constrained, the material element will still attempt to deform by Eq. (16). Following the classical weighted residual error method, the tendency for the material to reach the target strain rates can be expressed as

$$\int_V (\dot{\varepsilon}_{ij} - \dot{\varepsilon}_{exp}\delta_{ij})\,w_{ij}\,dV = 0 \tag{17}$$

in which the integration is over the entire volume of the sintering body and w_{ij} is a set of weight functions. Eq. (17) can be immediately reduced to Eq. (10) by choosing $w_{ij} = \delta\dot{\varepsilon}_{ij}$. This empirical statement of Eq. (17) does not rely on a linear constitutive law.

3. Case studies of DFEM

The DFEM proposed in this paper is an empirical method. Its validity can only be established using case studies. In this section, three cases studies are presented.

3.1. Case study A: dumb-bell shaped compact of alumina powder

This is a conceptional case study, instead of an experimental one, using a dumb-bell shaped compact of alumina powder as shown in Fig. 1. To create an extreme case of non-uniform sintering, an initial relative density of $D = 0.4$ is assigned to the top

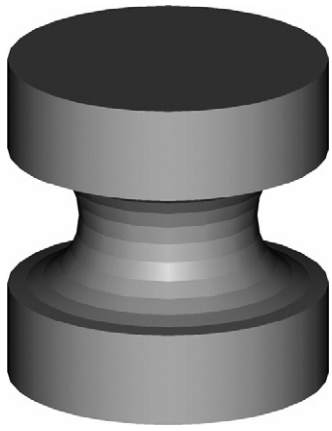

Fig. 1. The initial profile of an alumina powder compact used in case study A.

and the bottom parts of the component and $D = 0.7$ to the middle part as indicated in Fig. 2. The finite element mesh on the vertical cross-section of the component is shown in Fig. 2. Twenty-noded iso-parametric elements were used for a quarter of the component. Symmetric velocity boundary conditions were applied on the exposed internal boundaries. Only isothermal heating condition is considered. The problem is firstly solved using the usual finite element method and a full constitutive law described by Du and Cocks,[19] which is give by

$$\dot{\varepsilon}_{ij} = \frac{\dot{\varepsilon}_0}{\sigma_0}\left(\frac{d_0}{d}\right)^3 \left[\frac{3}{2}c(D)s_{ij} + 3f(D)(\sigma_m - \sigma_s)\delta_{ij}\right], \quad (18)$$

in which d_0 and d represent the initial and current grain-size, respectively, and c and f are the functions of the current and

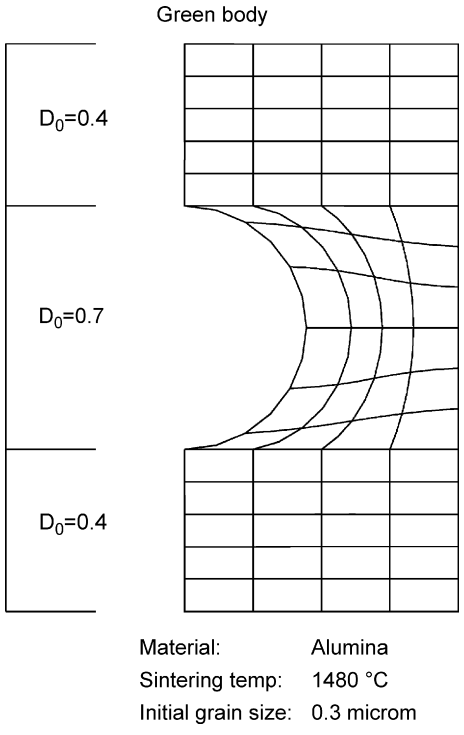

Fig. 2. The initial density distribution and finite element mesh shown on the cross-section of half the dumb-bell specimen.

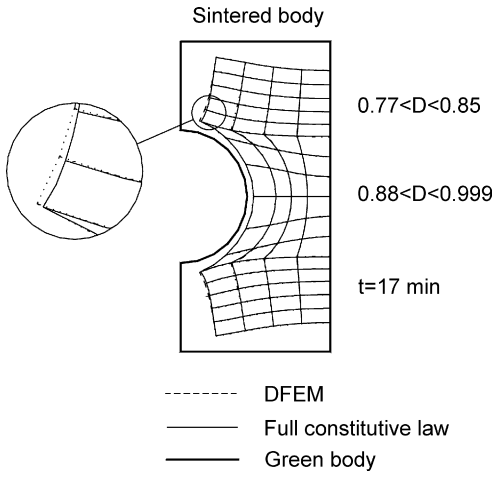

Fig. 3. Comparison of final shapes of the sintered dumb-bell specimen predicted by the finite element analysis using a full constitutive law (thin solid line) and the DFEM (dashed line), respectively. The outer solid line shows the initial shape of the green specimen.

initial relative density. Their detailed expressions were given in ref. 19. This constitutive law was intended for solid state sintering controlled by grain boundary diffusion. Du and Cocks[19] used $\sigma_0 = 3.33$ MPa, $\dot{\varepsilon}_0 = 4.53 \times 10^{-4}\ s^{-1}$ and $\sigma_s = 1$ MPa for a submicron alumina powder. These data were used in the current case study. Grain growth was not considered and the initial grain-size was set as $d_0 = 0.3$ μm. The same problem was then solved using the DFEM with the $\dot{\varepsilon}_{exp}$ calculated from Eq. (18) as

$$\dot{\varepsilon}_{exp} = -9\frac{\dot{\varepsilon}_0}{\sigma_0}\left(\frac{d_0}{d}\right)^3 f(D)\sigma_s \quad (19)$$

Fig. 3 compares the deformed shapes of the component obtained using the full constitutive law (solid line) and the DFEM (dashed lines) at $t = 1000$ s. The outer frame shown in the figure is the initial shape of the component. The component has been distorted severely showing that a large shear deformation as well as volume change has occurred. Yet there is only a small difference between the two results. A re-run of the case study considering grain growth showed the same accuracy of the DFEM.

3.2. Case study B: comparison with an experiment by Kim et al.[11]

In a case study to compare finite element analysis with direct experimental measurement, Kim et al.[11] compacted and sintered a complex shaped specimen of an alumina powder. Fig. 4 shows a quarter of their specimen with the finite element mesh used in the DFEM analysis. Kim et al.[11] determined the density distribution in the specimen after compaction by measuring Vickers hardness and the final geometry of the sintered specimen. They then carried out a finite element analysis for both the compaction and sintering processes. An empirical constitutive law was obtained using an experimental technique that the group had developed.[9–12] Fig. 5 reproduces their comparison of the sintered geometry predicted from the finite element

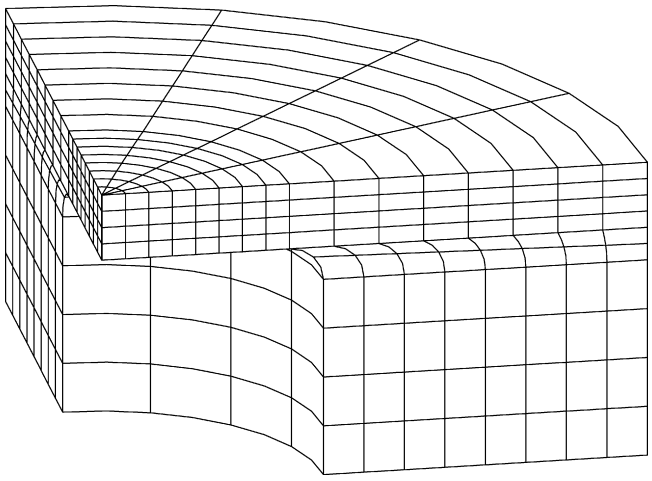

Fig. 4. The finite element mesh used in the DFEM analysis for case study B, which was analysed numerically and experimentally by Kim et al.[11]

method with the experimental measurement. This is a very careful study and the comparison perhaps represents the state-of-the-art of the current generation of finite element analysis for sintering.

In the current work, the sintering process was re-analysed using the DFEM and the densification data instead of the full constitutive law. The densification data of three different initial densities, $D_0 = 0.53, 0.59$ and 0.67, obtained by Kim et al.[11] were fitted using the quadratic shape functions[17] which are shown in Fig. 6. Linear interpolation and extrapolation were made to obtain densification curves for initial densities other than these three values. Twenty-noded iso-parametric elements were used. Only a quarter of the specimen was analysed due to the symmetry. Fig. 7 shows the comparison between the DFEM prediction and the experimental measurement. By comparing Figs. 5 and 7, it can be seen that the accuracy of the DFEM is comparable to that of the finite element analysis using a full constitutive law.

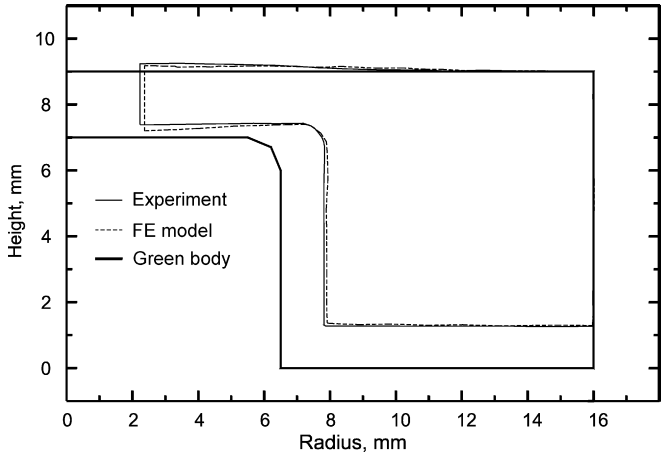

Fig. 5. Comparison of the final shapes of the sintered specimen obtained from the finite element model (dashed line) and experiment (thin solid line) by Kim et al.[11] The thick solid line shows the initial profile of the specimen. Reproduced from ref. 11.

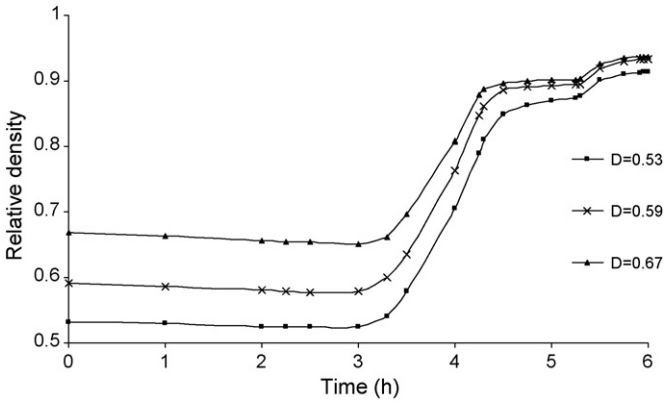

Fig. 6. Relative density as a function of time for three different initial densities obtained by Kim et al.[11] The data were fitted here using shape functions described in ref. 17 (solid lines) which were used in the current DFEM analysis.

3.3. Case study C: comparison with experiment using a mix of mineral raw materials

The dominating sintering mechanism for the two previous cases is solid state sintering controlled by grain boundary diffusion. To demonstrate the general applicability of the DFEM, a sintering experiment was performed at ENSCI using a ceramic body composition similar to porcelain, which is a mixture of kaolinitic clay, feldspar and quartz. During heating above 500 °C, the clay undergoes progressive phase transformations and at temperatures above about 1050 °C, incongruent melting of feldspar occurs. The sintering mechanism of the compact is complex, being dominated by the quantity and characteristics of the liquid phase.

A curved disc shaped specimen, as shown in Fig. 8, was shaped by uniaxial pressing in a metallic mould. Homogeneity and absence of flaws in the powder compact were ensured by a preliminary granulation operation and by optimisation of the pressing procedures. The compaction stress is different in different parts of the disc, leading to a density distribution within the compact. Local densities were determined from indentation sizes, using a specific indentation method at controlled rate and

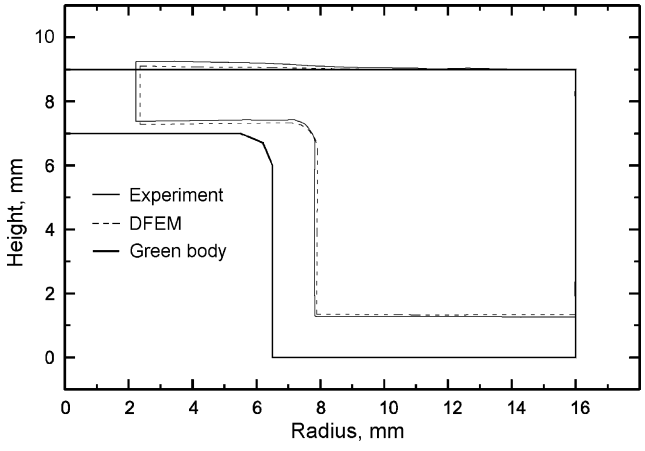

Fig. 7. Comparison of the final shapes of the sintered specimen obtained from the DFEM model (dashed line) in this work and experiment (thin solid line) of Kim et al.[11] The thick solid line shows the initial profile of the specimen.

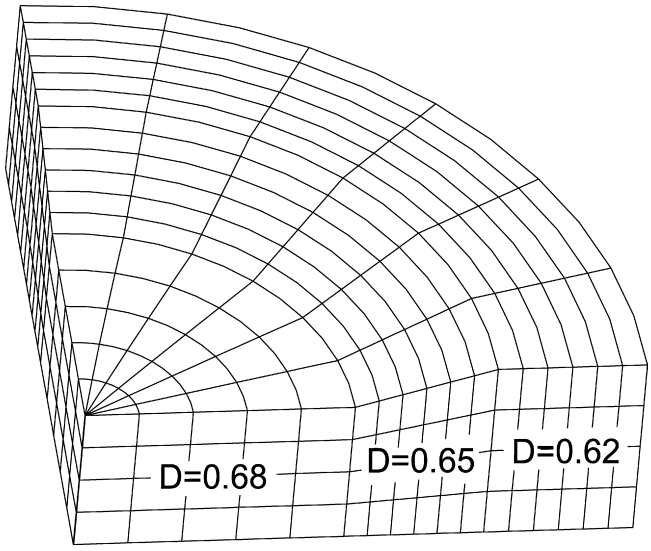

Fig. 8. The finite element mesh and initial density distribution for case study C.

load, and comparison with reference materials. In the DFEM it was assumed that the specimen had only three distinct initial densities as shown in Fig. 8. Using uniform samples of the three different initial densities, densification curves were obtained, as shown in Fig. 9. The measurements were carried out using dilatometry (Misura, Expert System Solution), with the same heating rate and time as for the sintered sample. The disc specimen was then sintered using a heating schedule of 7 °C min^{-1} up to 1250 °C then a cooling rate of 10 °C min^{-1} to room temperature. The final dimensions of the sintered disc were measured using a coordinate measuring system for three-dimensional measurements. The experimental accuracy of this measurement is 1%.

Figs. 10 and 11 compare the DFEM prediction with the experimental measurement for the final geometry of the disc specimen. The percentage errors of the dimensions at various locations are also shown in Fig. 11. Fig. 12 shows comparison between DFEM simulation and experimental result. It can be seen that the accuracy of the DFEM is quite acceptable, despite the uncertainties in input data in terms of the initial density dis-

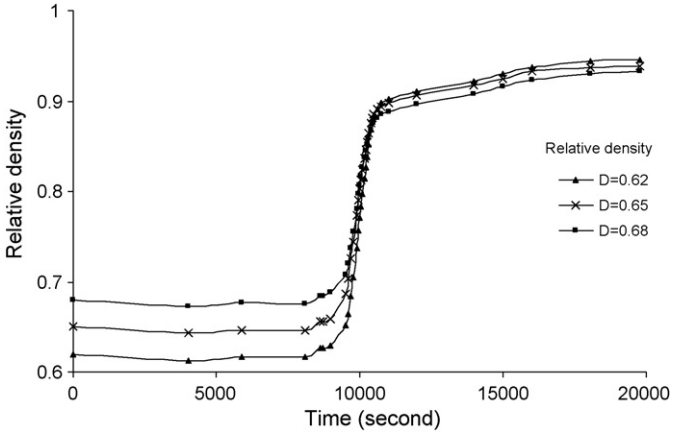

Fig. 9. Relative density as a function of time for the three different initial densities for case study C. These data were used in the DFEM analysis.

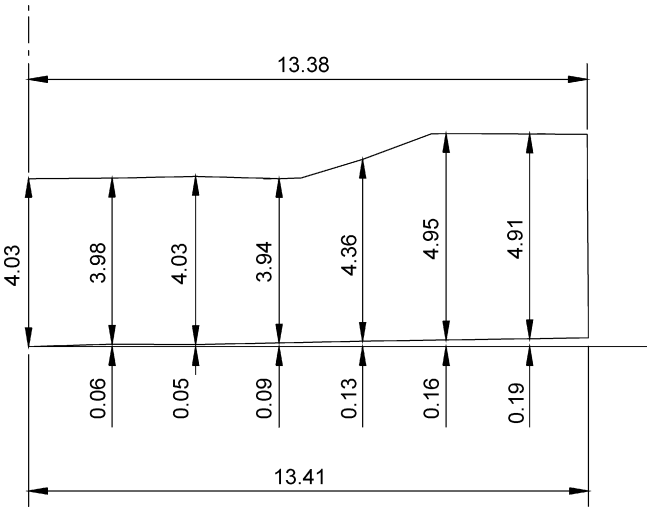

Fig. 10. Dimensions of the final shape of the saucer specimen in case study C as determined experimentally.

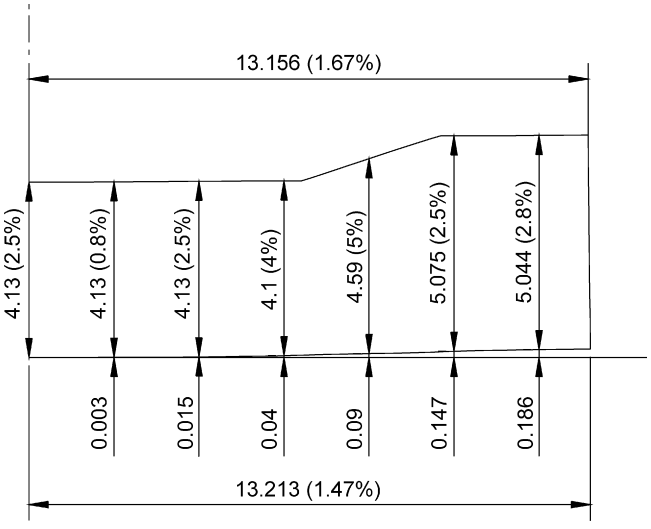

Fig. 11. Dimensions of the final shape of the saucer specimen in case study C predicted by the DFEM model. The percentage values in the brackets represent percentage errors compared with the experimental measurement as shown in Fig. 10.

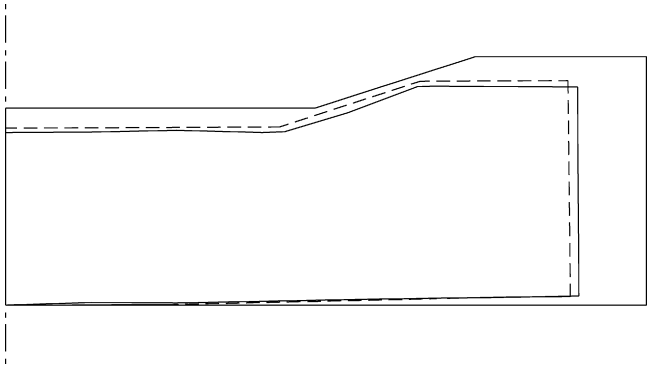

Fig. 12. Comparison of the final shapes of the sintered saucer specimen obtained from the DFEM model (dashed line) and experiment (thin solid line). The outer solid line shows the initial shape of the green specimen.

tribution and the complex phenomena involved in the sintering process.

4. Concluding remarks

The finite element technique is a powerful tool to accelerate the research and developed of sintered components. However, in a practical design cycle, it may be unrealistic to calibrate all the parameters in a constitutive law in order to carry out a full finite element analysis. For such problems the densification-based finite element method provides a cost-effective alternative for a proof of concept analysis. The method is not limited to any particular sintering mechanism and only requires densification data as its material input. The accuracy of the DFEM is comparable to the best that a full finite element analysis can currently achieve.

Acknowledgements

This work was partially supported by an EPSRC grant (S97996). Sasan Kiani acknowledges gratefully a partial Ph.D. studentship from the University of Surrey.

References

1. Cocks, A. C. F., The structure of constitutive laws for the sintering of fine grained materials. *Acta Metall.*, 1994, **42**, 2191–2210.
2. Olevsky, E. A., Theory of sintering: from discrete to continuum. *Mater. Sci. Eng.*, 1998, **R23**, 41–100.
3. Pan, J., Modelling sintering at different length scales. *Int. Mater. Rev.*, 2003, **48**, 69–85.
4. McMeeking, R. M. and Kuhn, l. T., A diffusional Creep law for powder compacts. *Acta Metal. Mater.*, 1992, **40**(5), 961–969.
5. Pan, J. and Cocks, A. C. F., A constitutive model for stage-2 sintering of fine grained materials—I. Grain-boundaries act as perfect sources and sinks for vacancies. *Acta Mater.*, 1994, **42**, 1215–1222.
6. Kraft, T. and Riedel, H., Numerical simulation of solid state sintering; model and application. *J. Eur. Ceram. Soc.*, 2004, **24**, 345–361.
7. Svoboda, J., Riedel, H. and Gaebel, R., A model for liquid phase sintering. *Acta Mater.*, 1996, **44**, 3215–3226.
8. McHugh, P. E. and Riedel, H., A liquid phase sintering model: application to Si_3N_4 and WC–Co. *Acta Mater.*, 1997, **45**, 2995–3003.
9. Gilla, O. *Phenomenological Modelling of the Behaviour of Sintering Materials and Numerical Modelling of Industrial Sintering of Cemented Carbide and Alumina* (Modelisation Phenomenologiquue de Comportment des Materiaux Frittants et Domulation Numerique du Frittage Industriel de Carbure Cemente D'Alumine). Ph.D. theses. INPG, France, January 2000.
10. Gilla, O., Josserond, C. and Bouvard, D., Viscosity of WC–Co compacts during sintering. *Acta Mater.*, 2001, **49**, 1413–1420.
11. Kim, H. G., Gilla, O., Doremus, P. and Bouvard, D., Near net shape processing of a sintered alumina. *Int. J. Mech. Sci.*, 2002, **44**, 2523–2539.
12. Kim, H. G., Gilla, O. and Bouvard, D., A phenomenological constitutive model for sintering of alumina powder. *J. Eur. Ceram. Soc.*, 2003, **23**, 1675–1685.
13. Tsvelikh, A., Thompson, W., Easton, A. and Freshwater, I., A geometrical finite element model of the sintering process of advanced ceramic compacts. *Comput. Mater. Sci.*, 1995, **3**, 457–464.
14. Ozkan, N. and Briscoe, B. J., Prediction of overall shape of sintered alumina compacts. *J. Eur. Ceram. Soc.*, 1994, **14**, 143–151.
15. Ozkan, N. and Briscoe, B. J., Overall shape of sintered alumina compacts. *Ceram. Int.*, 1997, **23**, 521–536.
16. DiAntonio, C. B., Ewsukand, K. G. and Bencoe, D. N., *Control of Low Temperature Co-Fire Ceramic Sintering, Sintering 2003*. Penn State University, Pennsylvania, September 15–17, 2003.
17. Kiani, S., Pan, J. and Yeomans, J. A., A new scheme of finding the master sintering curve. *J. Am. Ceram. Soc.*, in press.
18. Zienkiewicz, O. Z. and Taylor, R. L., *The Finite Element Method*. McGRAW-Hill Book Company, 1989.
19. Du, Z.-Z. and Cocks, A. C. F., Constitutive models for the sintering of ceramic components—I. Material models. *Acta Metal.*, 1992, **40**, 1969–1972.